Energy & Environmental Science

Accepted Manuscript

ROYAL SOCIETY OF CHEMISTRY

www.rsc.org/ees

Large Fill-Factor Bilayer Iodine Perovskite Solar Cells Fabricated by Low-Temperature Solution-Process

Qi Wang,[†] Yuchuan Shao[†], Qingfeng Dong[†], Zhengguo Xiao, Yongbo Yuan and Jinsong Huang[1]

Department of Mechanical and Materials Engineering and Nebraska Center for Materials and Nanoscience, University of Nebraska-Lincoln, Lincoln, Nebraska 68588-0656;

1. Introduction

Solution processed low cost, high efficiency photovoltaic devices have been persistently pursued in the past decade for renewable solar to electric energy conversion.[1-6] Recently, organolead halide perovskites have arisen as excellent earth abundant photovoltaic materials to compete with organic semiconductors[3,7] and quantum dots[6] due to their small bandgap, strong absorption, excellent crystallinity and long charge diffusion length.[4,8-21] They have been applied as active layer in both mesoporous structure and planar heterojunction (PHJ) solar cells with the highest demonstrated power conversion efficiency (PCE) exceeding 15%.[4,8-15] It has been recently revealed that halide perovskites have superior charge diffusion length to most solution-processed organic photovoltaic (OPV) and quantum-dot photovoltaic (QDPV) materials.[4,11,15] The balanced electron-hole diffusion lengths were found to approach the optical absorption length in solution-processed methylammonium lead iodide ($CH_3NH_3PbI_3$) and ten times longer than the optical absorption length in solution-processed $CH_3NH_3PbI_{3-x}Cl_x$.[4,11,15] Up to now, perovskite films have been formed by versatile film deposition approaches such as spin-coating[8,13,14], sequential deposition of the inorganic and organic precursor[9] and co-evaporation of

[1] Email address: jhuang2@unl.edu. [†]Q.W, Y.S and Q.D contributed to this work equally.

the precursors[10]. While low temperature spin-coating is among the simplest methods to fabricate low-cost solar cell devices, it was found very challenging to form continuous perovskite films by spin-coating the directly mixed lead iodine (PbI_2) and methylammonium halide blend precursor solution. [2,7,17,18,20] Non-fully covered perovskite films were frequently observed which might ascribe to the interaction of perovskite with substrate surface.[17,18] We observed very rough perovskite films with microfiber formation on perovskite films as shown in Figure 1a using the stoichiometry precursor solutions (molar ratio of PbI_2: methylammonium iodide (CH_3NH_3I)=1:1), leading to a large device leakage current as well as low fill factor (*FF*) and small open circuit voltage (V_{OC}) (Figure S1).

In this manuscript, we report a low-temperature solution process to form relatively continuous $CH_3NH_3PbI_3$ layer. It was found perovskite morphology is sensitive to precursor's composition variation and a non-stoichiometry precursor ratio could lead to a high device efficiency of 12.2%. The application of a spun conformal fullerene layer was found critical in avoiding leakage by covering the perovskite films and exposed anode area. Using a unique double fullerene layer structure to passivate the trap states, devices with a record *FF* of 80.1% were achieved for perovskite solar cells under one sun illumination.

2. Experiment

CH_3NH_3I was synthesized using the method described by Michael M. Lee, *et. al*.[8] A concentrated aqueous solution of hydroiodic acid (HI) (15.0 mL, 57 wt% in water, Alfa Aesar) was reacted with methylamine (CH_3NH_2) (13.5 mL, 40 wt% in aqueous solution, Alfa Aesar) at 0 °C for 2 h with constant stirring under nitrogen atmosphere. Methylammonium iodide was crystalized through removing the solvent by a rotary evaporator. The generated white powder was washed with diethyl ether (Alfa Aesar) three times and dried in vacuum overnight.

The indium tin oxide (ITO) substrates were cleaned and poly(3,4-ethylenedioxythiophene) poly(styrenesulphonate) (PEDOT:PSS) layer was spun on ITO as routine[1]. CH_3NH_3I and PbI_2 precursor were dissolved in anhydrous *N,N*-dimethylformamide (DMF) at different concentrations from 150 mg/ml to 350 mg/ml, and mixed at different ratios. The mixture solutions were spun onto PEDOT:PSS at a rate of 4,000 rounds per minute for 30 seconds. The perovskite films were annealed at 100 °C for 15-60 minutes. Here, the combination of a high precursor solution concentration and a high spin rate was used to reduce the roughness of the perovskite films. After the spin-coating of perovskite films, 30 nm C_{60} was thermal-evaporated with a deposition rate of 2-3 Å/s. The [6,6]-phenyl-C61-butyric acid methyl ester (PCBM) and indene-C_{60} bisadduct (ICBA) were dissolved in dichlorine benzine (DCB) at a concentration of 20~30 mg/ml were spun on the perovskite layer for some devices, which was followed by the low temperature annealing at 100 °C for 10~60 minutes. The highest efficiency devices have perovskite annealed at 100 °C for 60 minutes before ICBA coating, and 100 °C for 30 minutes after ICBA coating. The devices were finished by the evaporation of 7 nm 2,9-dimethyl-4,7-diphenyl-1,10-phenanthroline (BCP) and 100 nm aluminum electrode. The active device area (defined by the overlapping of ITO and aluminum electrode) is 0.06 cm^2.

Absorption spectra, photoluminescence (PL) spectra, scanning electron microscopy (SEM) pictures and X-ray diffraction (XRD) patterns of the films were recorded by Evolution 201 UV-Visible Spectrophotometer, iHR320 Photoluminescence Spectroscopy, Quanta 200 FEG Environmental Scanning Electron Microscope, and Rigaku D/Max-B X-ray diffractometer with Bragg-Brentano parafocusing geometry, respectively. It should be noted the perovskite films for XRD measurement were spun on PEDOT:PSS coated silicon substrates, giving the same compositions with real devices. The photocurrents of the devices were measured under AM1.5G

irradiation (100 mW/cm^2) with a xenon-lamp-based solar simulator (Oriel 67005, 150WSolar Simulator). A Schott visible-colour glass-filtered (KG5 colour-filtered) Si diode (Hamamatsu S1133) was used to calibrate the light intensity before photocurrent measurement.

3. Results and discussion

Our method of varying the precursor ratio in solution stems from the observation that two perovskite films formed on different surfaces are strikingly different in absorption and PL spectra, as shown in Figure 1b-c. These two films were spun on ITO and PEDOT:PSS from the same solution with PbI_2/CH_3NH_3I precursor molar ratio (defined as precursor ratio) of 0.7. It was speculated that the difference origins from the different affinities of the organic and inorganic precursors to the different surfaces. To verify it, we varied the precursor ratio from 0.35 to 1.0 to study the formation of perovskite on PEDOT:PSS which is the hole extraction layer in our devices. The absorption, PL, and XRD patterns were shown in Figure 1b-d as well to evaluate the formation of stoichiometric perovskite films. As shown in Figure 1b, the films with small amount of PbI_2 have a strong absorption peak in the UV range. Increased PbI_2 percentage in the precursor solution causes slightly red-shifted peak and enhanced absorption. Upon on an increased precursor ratio to 0.6, there is a distinct transition of absorption spectra patterns from strong absorption in UV-blue range to a broad absorption across the UV-visible range which indicates the formation of perovskite. The transition of absorption patterns with increased precursor ratio from 0.52 to 0.6 is associated with a PL peak shift from 750 nm to 765 nm, as shown in Figure 1c. When the precursor ratio is over 0.70, the PL peak is fixed at 770 nm which is close to that of the previously reported stoichiometry perovskite.[9] Further increasing PbI_2 ratio over 0.7 does not change the absorption and PL spectrum shape or the peak intensity. The PL and absorption peaks of the film spun on ITO with the precursor ratio of 0.7 are close to those of

the films on PEDOT:PSS with the precursor ratio of 0.56, indicating more PbI_2 content in the film spun on PEDOT:PSS. It might ascribe to better affinity of PbI_2 to the amphiphilic PEDOT:PSS than to ITO. XRD patterns in Figure 1d reveal tetragonal perovskite forms with small amount of PbI_2 added in the precursor solution, while impurity peaks disappear when the precursor ratio is over 0.6.[22] The non-unit precursor ratio for stoichiometric perovskite film formation indicates that the composition of the spun films is different from that in the precursor solution, which should attribute to the different affinities of CH_3NH_3I and PbI_2 to the substrates. The top surface SEM images of perovskite films with different precursor ratios are shown in Figure 1a. Increasing the amount of PbI_2 in the films generally increase the film roughness, and a lot of microfibers are observed when the precursor ratio is larger than 0.8. The tiled cross-section and top-view SEM image of perovskite film with precursor ratio of 0.78 (Figure 2a) showed distinct two-layer structures in the formed perovskite films: a flat, continuous bottom layer and a discontinuous top layer with many microstructures. The microstructures of the top layer vary dramatically with precursor ratios as shown in Figure 1a. It is not yet clear why such two-layer structures form but it is certainly related to the spin-coating process because the feature of the microstructures varies with different spin-coating parameters.

The typical structure used to evaluate the formed perovskite films is shown in Figure 2b which is similar to the PHJ OPVs.[23] It is noted that the a perforation in the perovskite film is sketched for better illustrating the working mechanism of our devices in the follow-up discussion. It does not indicate peroskite film is totally discontinous because the size of the hole is enlarged for clearity. A double layer fullerenes, with a spun PCBM or ICBA layer underneath followed by a thermal evaporated C_{60} layer, were used as electron extraction layer. BCP is a well-known electron transport/hole blocking layer which has been widely used in organic light emitting

diodes, organic photodetectors and organic photovoltaic devices. [24-28] Its functions have been thoroughly studied in OPVs including 1) blocking holes because of the poor hole mobility; 2) transporting electrons with large electron mobility; 3) reducing damage of the fullerene layer by followed metal deposition. To optimize the device performance, the composition and thickness of the $CH_3NH_3PbI_3$ films were tuned by varying the ratio and concentration of the precursor solutions, and different fullerene electron extraction layers were applied. Figure 3a shows composition dependent photocurrent curves for the devices fabricated by the same procedure except to the precursor ratio. In the devices with increased PbI_2 percentage, the more perovskite formed gives a larger short circuit current density (J_{SC}) due to the increased absorption, while the V_{OC} of the devices declines slightly. The films spun from solutions with precursor ratio larger than 0.8 often yielded non-working devices due to the large leakage current. This agrees with the morphology study by SEM (Figure 1a) that more PbI_2 in the films generally increase the roughness with a lot of microfibers showing up on the surface, possibly due to the crystallization of perovskite and/or PbI_2. The devices with precursor molar ratio of 0.6~0.7 have the largest PCE. This observation provides a plausible explanation for the previously reported low efficiency PHJ perovskite solar cells by solution process.

Figure 3b illustrates photocurrent of devices with different spun fullerene or fullerene derivatives. It is found the application of spun PCBM and ICBA significantly increase the V_{OC} of the perovskite photovoltaic devices. The device fabrication parameters of the three devices studied here were controlled to be the same except to the fullerene layers. The V_{OC} of the devices with perovskite coated by ICBA reaches 1.06 V which is 0.1~0.2 V larger than that of the device with PCBM interfacial modification, as shown in table 1. The V_{OC} enhancement in the devices

with spun PCBM or ICBA can be explained by the Schottky junction formed between the spun fullerene films and the underneath PEDOT:PSS layer which is described below.

A film thickness close to the charge diffusion length in the perovskite films is needed for strong absorption of light in red spectral range. The thicknesses of the devices with different precursor ratios were optimized, and the results were summarized in the Table I. A typical thickness dependent photocurrent of the devices with non-optimized annealing time of 15 minutes is shown in Figure 3c. The J_{SC} keeps increasing with the film thickness until a maximum of 14.0 mA/cm^2 is reached at the optimized perovskite thickness of 140 nm, and then reduces with the increased film thickness. Further increasing the film thickness to enhance the J_{SC} is likely hindered by the charge diffusion length in iodine perovskite which was reported to be around 100 nm.[11,15] The optimized precursor ratio increases from 0.60 to 0.78 with increased thickness of the perovskite layer, which can be explained that decreased affinity of PbI_2 to PEDOT:PSS for the material far away from the PEDOT:PSS surface. A larger percentage of PbI_2 in precursor solution is needed in the thick films to satisfy the stoichiometric composition. The film-thickness dependent V_{OC} variation behavior is different in devices with different fullerene layers. The V_{OC} remains almost invariant in the device with ICBA acceptor layer, while increases in the device with PCBM acceptor layer (Figure S2), which might be ascribed to the observed lower dark current in the thicker film devices.

The *FFs* of the perovskite devices are sensitive to composition and thickness of the perovskite layer as well as the electron extraction layers. The *FF* variation with precursor ratio exhibits a peak value in the molar ratio of 0.6, as shown in Table 1. A thinner perovskite layer also gives a larger *FF,* most likely due to more efficient collection of charges and reduced recombination in the thinner perovskite films. The *FF*s are also comparable for the devices with

PCBM and ICBA electron extraction layers, while a slightly larger *FF* of 80.1% is observed in the device with ICBA layers. This is in striking contrast to OPVs in which ICBA always yields a smaller *FF* than PCBM. To the best of our knowledge, the obtained *FF* is the highest among all the perovskite solar cells reported. The large *FF* and V_{OC} in our bilayer structure devices with ICBA layer indicate that the charge recombination limiting the efficiency in perovskite solar cells is different from that in OPVs or QDPVs.

The optimized devices have a precursor ratio of 0.6, thickness of 140 nm, and ICBA acceptor layer. Its thermal annealing time of perovskite film was optimized to 60 minutes under 100 ℃. Meanwhile, perovskite/ICBA layers were annealed 30 minutes at the same temperature. The highest efficiency device with photo- and dark- current shown in Figure 3d has a J_{SC} of 15.7 mA/cm^2, V_{OC} of 0.97 V, *FF* of 80.1% and PCE of 12.2%. It is expected the slight annealing after ICBA coating drives the diffusion of ICBA into the perovskite for a larger contact area. The performance of our high efficiency device didn't show reduction when it was tested with a mask to define the device area and avoid light piping (Figure S3). No obvious hysteresis of photocurrent was observed by changing the voltage sweep rates or direction (Figure S4).

It is noted that a very similar device structure was reported previously which also use PCBM or ICBA electron transport layer. Their reported V_{OC} of the device with C_{60} electron collection layer is comparable to what we have, but the V_{OC} of the PCBM or ICBA only devices are 0.3 to 0.4 V smaller than what were achieved in this work. And the *FF* reported here is much larger than previously reported. The huge improvement of device performance in this work can be explained by the unique double fullerene layer introduced in addition to a better controlling of active layer composition by varying precursor ratio. The first rewarding aspect for applying this double fullerene layer structure is the spun fullerene layer can effectively eliminate device

leakage. As above mentioned, rough perovskite top surfaces are generally observed in the SEM images, and devices fabricated by these films often exhibit large leakage current. It is therefore speculated there is still exposed PEDOT:PSS area which is not fully covered by perovskite. The spun fullerene layer must cover the exposed PEDOT:PSS area by forming a conformal layer, which is evidenced by the SEM image of perovskite film covered by a spun ICBA layer as shown in Figure 4a-c. This conformal fullerene covering effectively eliminates the leakage current. To verify this speculation, we made devices with or without solution processed fullerene layer:

Device I: ITO/ PEDOT:PSS/Perovskite (140 nm)/C_{60} (50 nm, thermal-evaporated)/BCP/Al

Device II: ITO/ PEDOT:PSS/Perovskite (140 nm)/C_{60} (20 nm, spun)/C_{60} (30 nm, thermal evaporation)/BCP/Al

Figure 4d shows the dark current curves of the devices with and without a spun C_{60} layer. The device without a spun C_{60} layer exhibits a huge leakage current density larger than 10 mA/cm^2 even under a small reverse bias of 0.1 V. Nevertheless, after inserting a spun C_{60} layer onto the perovskite, the dark current is dramatically reduced by 3-4 orders of magnitude, demonstrating a spun fullerene layer is crucial in preventing leakage. In order to find out whether the solvent of fullerene played a role in reducing leakage, we also made devices with DCB washed perovskites. No obvious morphology change of the perovskite film surface was observed in SEM images of before and after DCB washing (Figure 4a, Figure S5). Meanwhile, the dark current of the devices fabricated by DCB washed perovskite films still shows large leakage, although it was reduced by several times (Figure 4d). As the DCB wash effect, though exists, is

relatively minor, we then explain it is the spun fullerene forms a conformal layer that cover most of the perovskite surface to prevent leakage.

The contact of fullerenes with PEDOT:PSS forms Schottky junction, which was discovered by us previously.[29] Consequently, our devices consist of two type of devices, perovskite/fullerene PHJ devices and PEDOT:PSS/fullerene Schottky junction devices, connected in parallel. This scenario is sketched in the device structure of Figure 2b. The overall V_{OC} is determined by both perovskite cell and the Schottky junction cell based on their relative cell area. The contact of PCBM and ICBA with PEDOT:PSS should not compromise the V_{OC} of the whole devices because a large V_{OC} around of 0.87 V and 0.95 V can be obtained from the PCBM/PEDOT:PSS and ICBA/ PEDOT:PSS Schottky junction devices.[29] However, if C_{60} is spun onto perovskite, the devices overall V_{OC} was reduced to ~0.5 V because V_{OC} of C_{60}/PEDOT:PSS Schottky junction is only around 0.45 V. [29]

The other important role this double fullerene layer structure plays is its better passivation effect of traps in perovskite. To verify this scenario, we conducted thermal admittance spectroscopy (TAS) to quantitatively analyze the passivation of perovskite by PCBM and C_{60}.[30] TAS is a well-established technique for determination of the defect density of states which has been broadly applied in understanding defects in the thin film solar cells and organic solar cells.[31, 32] The trap density of states (tDOS) distribution can be derived from the angle frequency dependent capacitance via,

$$N_T(E_\omega) = -\frac{V_{bi}}{qW}\frac{dC}{d\omega}\frac{\omega}{k_B T}$$

where V_{bi} is the built-in potential, q is the element charge, W is the depletion width, C is capacitance, ω is the applied angular frequency, k_B is the Boltzmann's constant, T is the

temperature. V_{bi} and W were extracted from the capacitance-voltage measurement. The applied angular frequency ω defines the energy demarcation,

$$E_\omega = k_B T ln(\frac{\omega_0}{\omega})$$

The trap states below the energy demarcation can capture or emit charge with the given ω and contribute to the capacitance while the defect states above the energy demarcation cannot. Thus the frequency differential capacitance measurements provide the distribution of tDOS, which are performed by the E4980A Precision LCR Meter from Agilent at frequency between 0.1 to 1000 kHz.

The results in Figure 4e show that the devices without any fullerene layer have a relatively large trap density between 1×10^{17} and 1×10^{19} $m^{-3}eV^{-1}$ (black square) which is detrimental to the device performance. Three trap bands can be identified as labeled in the figure (separated by red dot lines). After depositing the C_{60} or PCBM layer, the tDOS reduced dramatically, indicating that both the C_{60} and PCBM effectively passivated the defects in perovskite films. It is noticed that C_{60} and PCBM have different but complementary passivation capability to the different trap bands. PCBM prefers to passivate the trap states in Band 2 (0.40~0.50 eV) and C_{60} has a stronger passivation effect on trap states with trap depth larger than 0.50 eV (Band 3). The tDOS of the device with PCBM and C_{60} double fullerene layers with optimum thermal annealing time is smaller than those with either PCBM or C_{60}, and is about two orders of magnitude lower than the device without fullerenes in the whole defect spectral range. This result demonstrated that the PCBM and C_{60} cooperate with each other well and further reduce the trap densities. This explains the better device performance, especially the record *FF*, in our optimized devices with double fullerene layers.

4. Conclusion

In summary, we reported the 12.2% iodine perovskite solar cell devices fabricated by a low temperature solution process with a simple bilayer device structure. Our finding of substrate surface sensitive perovskite composition is critical in the design and fabrication of other solution processed perovskite photovoltaic devices, especially chlorine containing perovskite materials which have a ten times longer electron-hole diffusion length. The double fullerene layer structure is expected to find its broad application in many other perovskite devices with its excellent passivation effect.

Acknowledgements: The authors thank the financial support by the National Science Foundation under Awards ECCS-1201384 and ECCS-1252623 and the Nebraska Public Power District through the Nebraska Center for Energy Sciences Research.

Figure Legends:

Figure 1. *Top view SEM images (a), absorption spectra (b), PL spectra (c) and XRD patterns (d) of the iodine perovskite films spun from solutions with precursor ratio from 0.35 to 1. All the perovskite films in b-c were spun on PEDOT:PSS expect the ones that are labeled as on ITO. Precursor ratio of the perovskite films spun on ITO is 0.7. The scale bar of SEM images are 2 μm in sample with precursor ratio of 0.6 and 3 μm for all others. The absorbance spectra are shifted by 2 with respect to each other, and the PL spectra are normalized and shifted with respective to each precursor composition for clarity. The vertical dashed lines in the absorption spectra and PL spectra, which show the reported absorption band edge and PL peak of iodine perovskite respectively, are added for eye guidance.*

Figure 2. *(a) Tilted cross-section SEM image of perovskite film spun from solution with precursor ratio of 0.78. The continuous perovskite layer (CPL) and microstructure perovskite layer (MPL) are labeled. The scale bar is 1 μm; (b) Schematic device structure of the perovskite PV devices. ICBA or PCBM layer was sketched as a conformal layer and the two types of junction were also depicted. The thickness of the each layer was not in scale with the real thickness for clarity.*

Figure 3*. The photocurrents of the devices under AM 1.5 simulated illumination with different precursor ratio (a), different acceptor layer (b), and different thickness (c). The devices in (a) have a thickness of 140 nm and ICBA acceptor layer; The devices in (b) have a precursor ratio of 0.6 and thickness of 75 nm. The devices in (c) have a precursor ratio of 0.6 and ICBA acceptor layer. (d) The photo- and dark- currents of the highest efficiency device.*

Figure 4 *(a) Top view of SEM image of the as-spun perovskite film. (b) Top view SEM image of perovskite film after ICBA spin-coating. The perovskite films in a-b were spun from the solution*

with precursor ratio of 0.6 and concentration of 250 mg/ml. The scale bar is 500 nm. (c) Cross-section SEM of a working device with a thin (75 nm) perovskite layer. (d) Dark current of perovskite devices with different fullerene layer fabrication processes. Black square, red circle, blue triangle curves are for the devices with 50 nm C_{60}, perovskite film washed by DCB solvent, 20 nm spun C_{60} plus 30 nm evaporated C_{60}, respectively. (e) Trap density of states (tDOS) for devices passivated by single PCBM layer (blue triangle), single C_{60} layer (red dot), PCBM/C_{60} double fullerene layers (grey star); Black square represents the device without fullerene passivation.

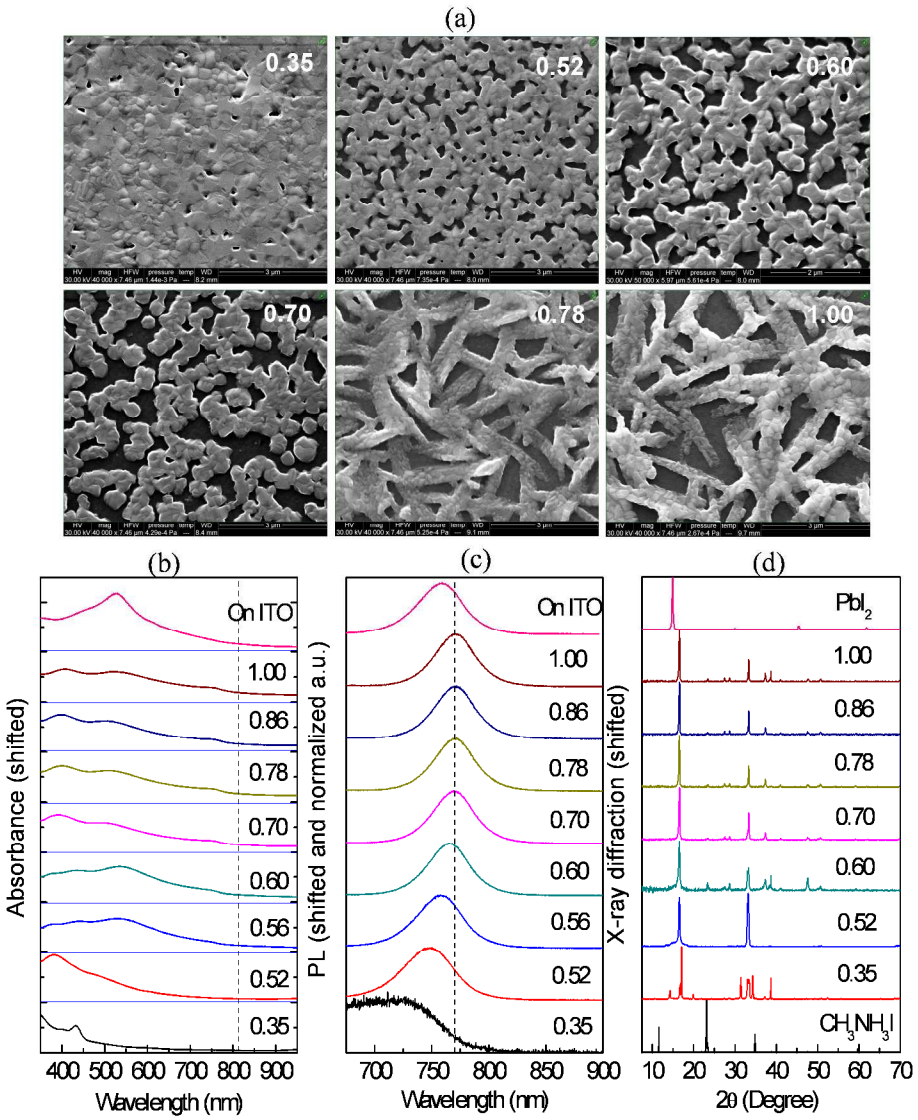

Figure 1. ***Q. Wang et al***

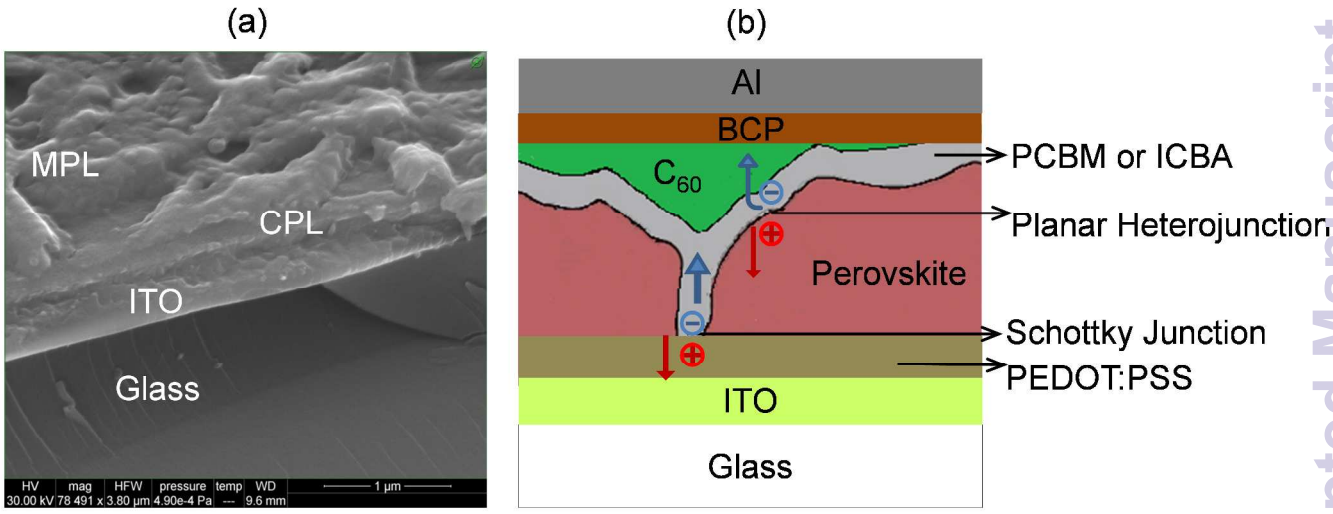

Figure 2. ***Q. Wang et al***

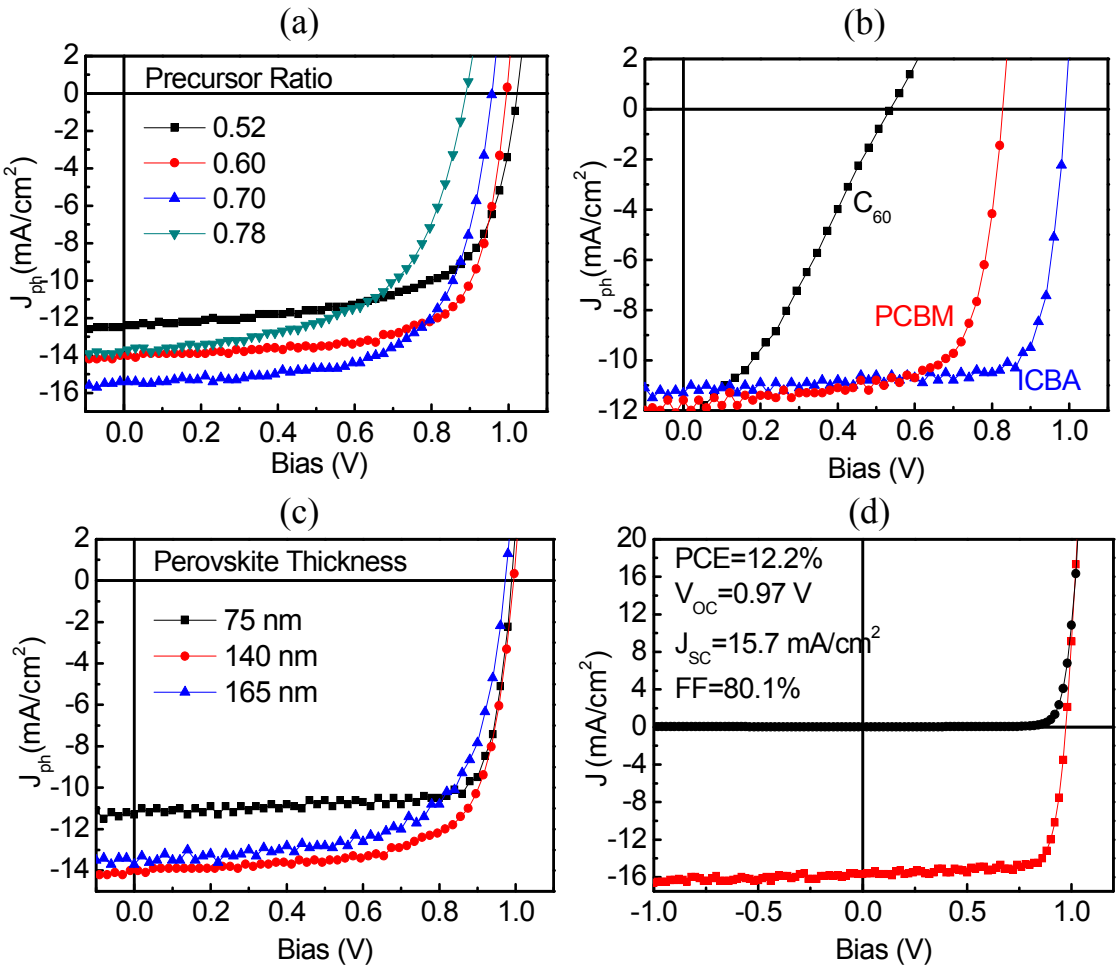

Figure 3. ***Q. Wang et al***

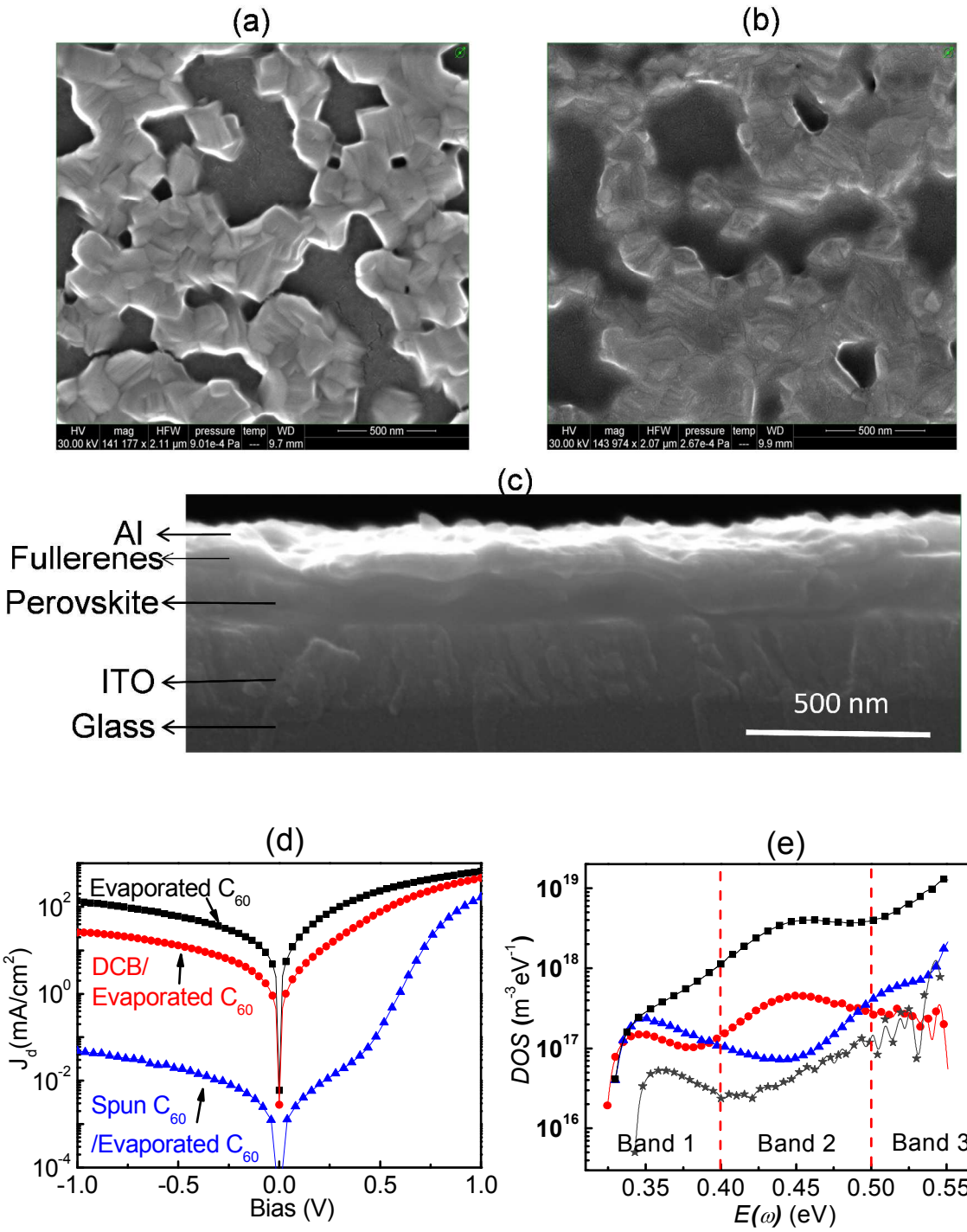

Figure 4. ***Q. Wang et al***

Table 1 Performance of devices with different precursor molar ratio, perovskite thicknesses and fullerene derivative layers

Device structure	Perovskite thickness	Precursor molar ratio	J_{SC} (mA/cm^2)	V_{OC} (V)	FF (%)	PCE (%)
ITO/ PEDOT:PSS /Perovskite/PCBM/ C_{60}/BCP/AL	75 nm	0.60	12.4	0.82	74.1	7.53
		0.70	11.2	0.86	73.7	7.1
		0.78	10.4	0.87	74.7	6.76
		0.86	9.97	0.88	74.1	6.50
	100 nm	0.60	11.9	0.91	67.2	7.28
		0.70	14.2	0.86	60.4	7.38
		0.78	12.7	0.89	67.6	7.64
		0.86	14.5	0.89	71.4	9.22
	140 nm	0.52	13.5	0.9	64.9	7.89
		0.60	15.3	0.86	57.3	7.54
		0.78	15.9	0.88	72.2	10.1
		0.86	16.3	0.8	60.8	7.93
ITO/ PEDOT:PSS /Perovskite/ICBA/ C_{60}/BCP/AL	75 nm	0.60	11.3	0.98	80.0	8.83
	140 nm	0.52	12.5	1.02	63.8	8.14
		0.60	14.0	0.99	71.1	9.85
		0.60	15.7	0.97	80.1	12.2
		0.70	15.4	0.96	65.3	9.66
		0.78	13.8	0.88	58.9	7.15
	165 nm	0.43	7.05	1.06	47.5	3.55
		0.52	9.13	1.05	55.8	5.35
		0.60	13.7	0.98	64.4	8.65
		0.70	15.3	0.94	46.6	6.70
		0.78	14.1	0.93	68.4	8.97
ITO/ PEDOT:PSS /Perovskite/C_{60}/BCP/AL	75 nm	0.60	12.2	0.53	33.1	2.14

Supplementary Information

Efficient Bilayer Iodine Perovskite Solar Cells by Low-Temperature Solution-Process

*Qi Wang,[†] Yuchuan Shao[†], Qingfeng Dong[†], Zhengguo Xiao, Yongbo Yuan and Jinsong Huang**

Department of Mechanical and Materials Engineering and Nebraska Center for Materials and Nanoscience, University of Nebraska-Lincoln, Lincoln, Nebraska 68588-0656;

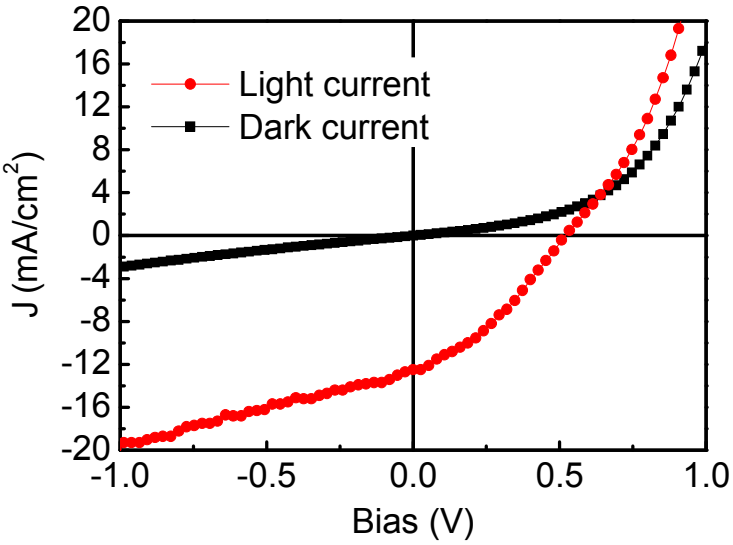

Figure S1 The photo- and dark-current of device fabricated by precursor molar ratio of PbI_2: CH_3NH_3I=1:1

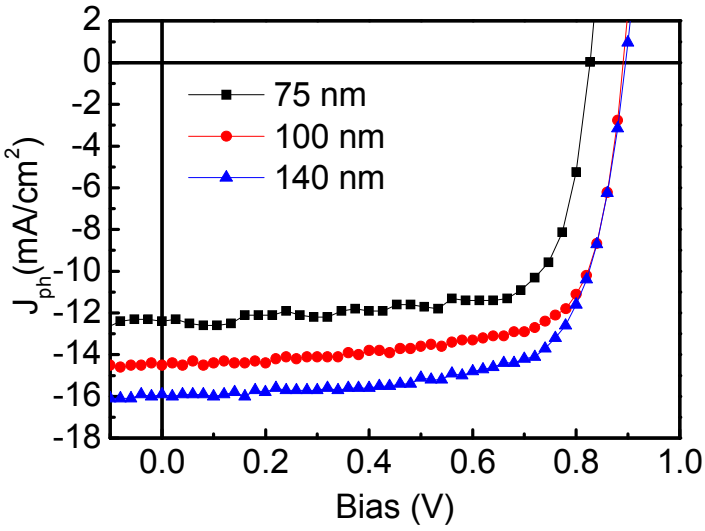

Figure S2 The photocurrents of the devices under AM 1.5 simulated illumination with different film different thicknesses. The devices have a precursor ratio of 0.6 and acceptor layer of PCBM.

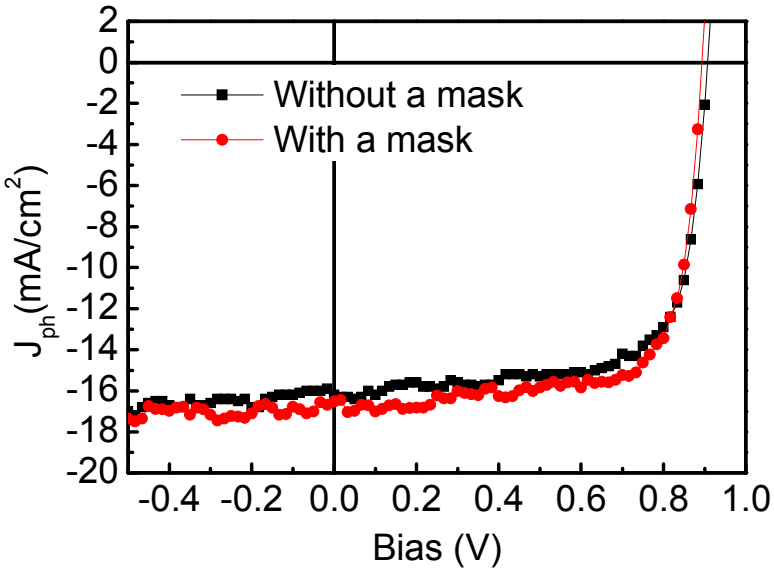

Figure S3 The photocurrent of a high performance perovskite device with or without a mask. The photocurrent was tested under AM 1.5 simulated illumination.

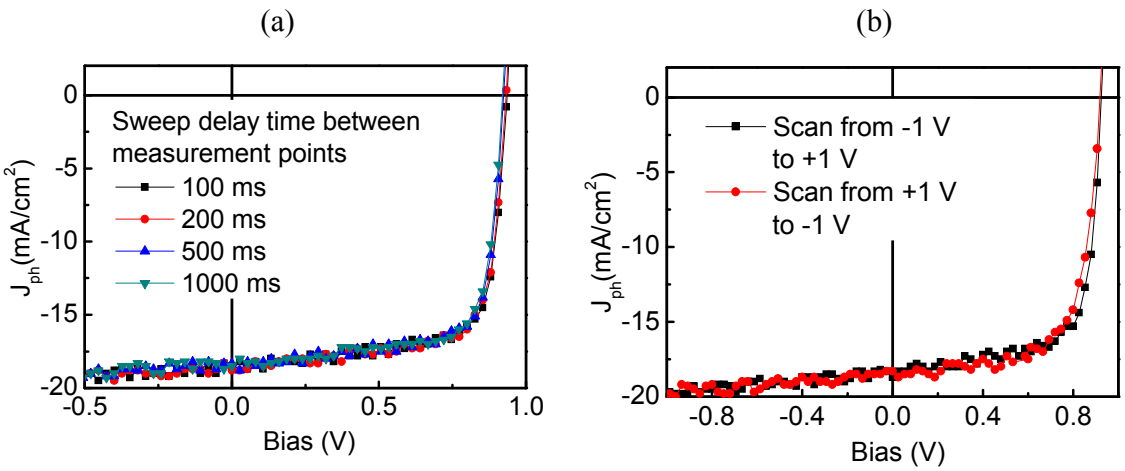

Figure S4 Photocurrents of a high performance perovskite device measured with different delay between measurement points (a) and different sweep directions (b). The photocurrent was tested under AM 1.5 simulated illumination.

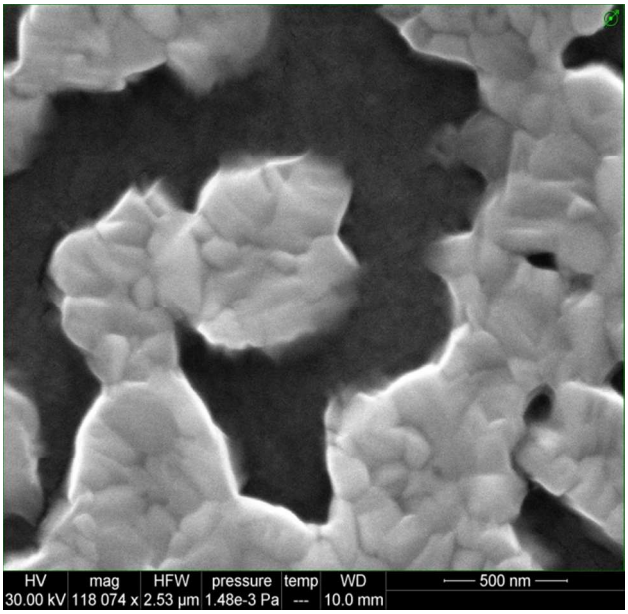

Figure S5 Top view SEM images of perovskite film after DCB wash. The perovskite film was spun from the solution with precursor ratio of 0.6 and concentration of 250 mg/ml. The scale bar is 500 nm.

Reference:

1. Y. B.Yuan, T. J. Reece, P. Sharma, S. Poddar, S. Ducharme, A. Gruverman, Y. Yang and J. S. Huang, *Nat. Mater.,* 2011, **3**, 296-302
2. I. Chung, B. Lee, J. He, R. P. H. Chang and M. G. Kanatzidis, *Nature*, 2012, **485**, 486-490
3. G. Li, R. Zhu and Y. Yang, *Nat. Photon.,* 2012, **6**, 153-161
4. G. Hodes, *Science,* 2013, **342**, 317-318
5. Y. M. Sun, G. C.Welch,W. L. Leong, C. J. Takacs, G. C. Bazan and A. J. Heeger, *Nat. Materi.,* 2012, **11**, 44-48
6. A. H. Ip, S. M. Thon, S. Hoogland, O. Voznyy, D. Zhitomirsky, R. Debnath, L. Levina, L. R. Rollny, G. H. Carey, A. Fischer. K. W. Kemp, I. J. Kramer, Z. Ning, A. J. Labelle, K. W. Chou, A. Amassian and E. H. Sargent, *Nat. Nanotechnol.,* 2012, **7**, 577-582
7. S. H. Park, A. Roy, S. Beaupre, S. Cho, N. Coates, J. S. Moon, D. Moses, M. Leclerc, K. Lee and A. J. Heeger, *Nat. Photon.,* 2009, **3**, 297-303.
8. M. M. Lee, J. Teuscher, T. Miyasaka, T. N. Murakami and H. J. Snaith, *Science,* 2012, **338**, 643-647.
9. J. Burschka1, N. Pellet, S. J. Moon, R. H. Baker, P. Gao, M. K. Nazeeruddin and M. Gratzel, *Nature,* 2013, **499**, 316-320
10. M. Z. Liu, M. B. Johnston and H. J. Snaith, *Nature,* 2013, **501**, 395-398
11. S. D. Stranks, G. E. Eperon, G. Grancini, C. Menelaou, M. J. P. Alcocer, T. Leijtens, L. M. Herz, A. Petrozza and H. J. Snaith, *Science,* 2013, **342**, 341-344
12. H. J. Snaith, *J. Phys. Chem. Lett.,* 2013, **4**, 3623-3630
13. A. Kojima, K. Teshima, Y. Shirai and T. Miyasaka, *J. Am. Chem. Soc.,* 2009, **131**, 6050-6051

14. J. Y. Jeng, Y. F. Chiang, M. H. Lee, S. R. Peng, T. F. Guo, P. Chen and T. C. Wen, *Adv. Mater.,* 2013, **25**, 3727-3732
15. G. C. Xing, N. Mathews, S. Y. Sun, S. S. Lim, Y. M. Lam, M. Gratzel, S. Mhaisalkar and T. C. Sum, *Science,* 2013, **342**, 344-347
16. J. H. Im, C. R. Lee, J. W. Lee, S. W. Park and N. G. Park, *Nanoscale,* 2011, **3**, 4088-4093.
17. A. Abrusci, S. D. Stranks, P. Docampo, H. L. Yip, A. K. Y. Jen and H. J. Snaith, *Nano Lett.,* 2013, **13**, 3124-3128
18. M. J. Carnie, C. Charbonneau, M. L. Davies, J. Troughton, T. M. Watson, K. Wojciechowski, H. Snaith and D. A. Worsley, *Chem. Commun.,* 2013, **49**, 7893-7895.
19. H. S. Kim, I. M. Sero, V. G. Pedro, F. F. Santiago, E. J. J. Perez, N. G. Park and J. Bisquert, *Nat. Commun.,* 2013, **4**, 2242
20. N. G. Park, *J. Phys. Chem. Lett.,* 2013, **4**, 2423-2429
21. W. Zhang, M. Saliba, S. D. Stranks, Y. Sun, X. Shi, U. Wiesner and H. J. Snaith, *Nano lett.,* 2013, **13**, 4505-4510.
22. T.Baikie, Y. Fang, J. M. Kadro, M Schreyer, F. Wei, S. G. Mhaisalkar, M Graetzeld and T. J. White, *J. Mater. Chem. A,* 2013, **1**, 5628-5641
23. V. I. Adamovich, S. R. Cordero, P. I. Djurovich, A. Tamayo, M. E. Thompson, B. W. DAndrade and S. R. Forrest, *Org. Electron.,* 2003, **4**, 77-87
24. P. Peumans and S. R. Forrest, *Appl. Phys. Lett.,* 2001, **79**, 126-128
25. P. Peumans, V. Bulovic, and S. R. Forrest, *Appl. Phys. Lett.,* 2000, **76**, 2650-2652
26. F. W. Guo, B. Yang, Y. B. Yuan, Z. G. Xiao, Q. F. Dong, Y. Bi and J. S. Huang, *Nat. Nanotechnol*, 2012, **7**, 798-802
27. F. W. Guo , Z. G. Xiao and Jinsong Huang, *Adv. Optical. Mater.*, 2013, **1**, 289–294

28. P. Peumans, A. Yakimov and S. R. Forrest, *J. Appl. Phys.,* 2003, **93**, 3693-3723
29. B. Yang, F. W. Guo, Y. B. Yuan, Z. G. Xiao, Y. Z. Lu, Q. F. Dong and J. S. Huang, *Adv. Mater.,* 2013, **25**, 572-577.
30. T. Walter, R. Herberholz, C. Muller and H. W. Schock, *J. Appl. Phys.*, 1996, **80**, 4411-4420
31. U. Rau, D. A. Ras and T. Kirchartz, Advanced characterization techniques for thin film solar cells, John Wiley & Sons, 2011
32. S. Khelifi, K. Decock, J. Lauwaert, H. Vrielinck, D. Spoltore, F. Piersimoni, J. Manca, A. Belghachi and M. Burgelman, *J. Appl. Phys.*, 2011, **110**, 094509